Journal of Computational Physics **170,** 764–784 (2001)
doi:10.1006/jcph.2001.6760, available online at http://www.idealibrary.com on IDEAL®

Numerical Simulation of Grain-Boundary Grooving by Level Set Method

M. Khenner,* A. Averbuch,* M. Israeli,† and M. Nathan‡

**School of Computer Science, Tel Aviv University, Tel Aviv 69978, Israel; †Faculty of Computer Science, Technion, Haifa 32000, Israel; and ‡Department of Electrical Engineering–Physical Electronics, Faculty of Engineering, Tel Aviv University, Tel Aviv 69978, Israel*
E-mail: amir@math.tau.ac.il

Received July 10, 2000; revised February 2, 2001

A numerical investigation of grain-boundary grooving by means of a level set method is carried out. An idealized polycrystalline interconnect which consists of grains separated by parallel grain boundaries aligned normal to the average orientation of the surface is considered. Initially, the surface diffusion is the only physical mechanism assumed. The surface diffusion is driven by surface-curvature gradients, while a fixed surface slope and zero atomic flux are assumed at the groove root. The corresponding mathematical system is an initial boundary value problem for a two-dimensional equation of Hamilton–Jacobi type. The results obtained are in good agreement with both Mullins analytical "small-slope" solution of the linearized problem (W. W. Mullins, 1957, *J. Appl. Phys.* **28**, 333) (for the case of an isolated grain boundary) and with the solution for a periodic array of grain boundaries (S. A. Hackney, 1988, *Scripta Metall*. **22**, 1731). Incorporation of an electric field changes the problem to one of electromigration. Preliminary results of electromigration drift velocity simulations in copper lines are presented and discussed.

1. INTRODUCTION

This paper presents the results of our work on numerical modeling and simulation of grain-boundary (GB) grooving by surface diffusion. Our ultimate goal is to develop and test a fast numerical approach for the simulation of the formation development propagation of groove-like defects in thin film interconnects used in microelectronics (ME).

In the modern ME industry, the quality and reliability of ME integrated circuits (ICs) have become no less important than their performance. Some of the most vulnerable elements of ME ICs, susceptible to several types of mechanical failures, are the interconnects. These are metallic conductors which connect the active elements.

0021-9991/01 $35.00

The defects (due to the small cross-section, high current density, mechanical stresses, and presence of GBs acting as fast diffusion pathways) lead to the loss of electrical and mechanical integrity, i.e., to line opens or shorts. Thus, such defects are one of the main reliability concerns in advanced integrated circuits.

1.1. *Mechanisms of Mechanical Failure in Interconnect Lines*

In this section we describe some basic failure mechanisms in interconnects and outline an appropriate physical model.

Many properties of polycrystalline materials are affected by the intersection of GBs with external surfaces, especially in the presence of applied or internal fields. Common examples are growth of GB grooves and cavities [13, 14], stress voiding [31], and electromigration (EM) [2, 15, 21, 25].

In the absence of an external potential field, the GB atomic flux $I_{GB} = 0$, and the corresponding groove profile evolves via surface diffusion under well-known conditions of scale and temperature (the so-called Mullins problem [17]). Mass transport by surface diffusion is driven by the surface Laplacian of curvature. Essentially for convex surfaces, matter flows from high-curvature regions, while for concave surfaces the flow is from low-curvature regions. To solve surface-diffusion problems, four different approaches have been taken. We refer the interested reader to the article by Zhang and Schneibel [32], where these approaches are discussed, and to the references therein.

The physical origins of a GB flux may be gradients of the normal stress at grain boundaries [8] and/or electromigration forces [3]. GB grooving with a GB flux in real thin film interconnects is a complex problem. It requires a sophisticated numerical modeling technique which can manage with such issues as aperiodic arrays of GBs, anisotropy of the surface tension, GB migration, formation of slits with a local steady-state shape in the near-tip region, and bridging across the slits near their intersections with the surface left behind [21]. The level set (LS) method seems to be a good candidate for addressing the problems; however, it has never been used for this purpose. As the first step in application of the LS method to the problem of grooving with an EM flux, we test in this paper the LS method over two simple—and already solved—grooving problems, and compare the results of LS method with those in [10, 17]. The first problem is the classical Mullins problem (GB grooving controlled by surface diffusion in an infinite bicrystal with a stationary GB). The second is GB grooving by surface diffusion in a periodic GB array of stationary GBs. Finally, we show the incorporation of an electric field as a driving force (the electromigration problem) and present preliminary results which show extremely good correlation with experimental data.

Below we give more details of the physical model.

The Mullins problem—Driving forces and diffusion mobilities. In the absence of an electric current, the diffusion is driven by a variation in chemical potential, μ_s, which causes atoms to migrate from high-potential to low-potential regions. It may be shown that [17]

$$\mu_s = K_s \gamma_s \Omega, \tag{1.1}$$

where K_s is the surface curvature, γ_s is the surface tension, and Ω is the atomic volume. Gradients of chemical potential are therefore associated with gradients of curvature.

In interconnects, GBs represent numerous fast diffusion pathways with a high diffusion coefficient, D_{gb}. As a matter of fact, the bulk diffusion can be neglected [17]. The diffusion

flux along the GB, J_{gb}, is given by

$$J_{gb} = \frac{D_{gb}\delta_{gb}}{kT}\nabla\mu_s, \tag{1.2}$$

where δ_{gb} is the GB thickness, k is the Boltzmann constant, and T is the absolute temperature.

Let τ be the tangential direction to the surface profile in 2D. If $\mathbf{n} = (n_x, n_y)$ is the unit vector normal to the surface or GB, then the following relations hold:

$$\tau = (n_y, -n_x), \quad \frac{\partial K_s}{\partial \tau} = \nabla K_s \cdot \tau = \frac{\partial K_s}{\partial x} n_y - \frac{\partial K_s}{\partial y} n_x \equiv K_\tau^s. \tag{1.3}$$

The surface-diffusion flux along the groove walls (volume crossing unit length per unit time) is given by

$$J_s^{\nabla K_s} = -\frac{D_s\delta_s}{kT}\frac{\partial \mu_s}{\partial \tau} = -BK_\tau^s, \tag{1.4}$$

where the superscript indicates that the flux is due to the curvature gradient,

$$B = \frac{D_s\delta_s\gamma_s\Omega}{kT} \tag{1.5}$$

is known as Mullins constant, and D_s, δ_s, k, and T denote surface-diffusion coefficient, thickness of the surface-diffusion layer, Bolzmann's constant, and absolute temperature, respectively. Note that $J_s^{\nabla K_s}$ is proportional to the first directional derivative of the curvature.

Physical boundary condition at the groove root. This boundary condition is dictated by the local equilibrium between the surface tension, γ_s, and the GB tension, γ_{gb}. In the symmetric case of a GB ($x = 0$) normal to an original ($y = \text{const.}$) flat surface, the angle of inclination of the right branch of the surface at the groove root with respect to the x axis is [17] (see Fig. 1)

$$\theta_0 = \sin^{-1}(\gamma_{gb}/2\gamma_s) = \text{const.} \tag{1.6}$$

The rapid establishment of the equilibrium angle between the GB and the surface by atomic migration in the vicinity of the intersection develops some curvature gradient at the adjacent surface and thus induces a surface-diffusion flux along the groove wall in the direction away from the groove root, opposite to the groove extension direction.

2. MATHEMATICAL MODEL

2.1. *The Conventional Approaches*

An adequate mathematical model which captures the above physical phenomena in interconnects was first developed by Mullins [17] and further extended by him and others [13, 14, 18]. It describes the evolution of the groove shape, $y(x, t)$ and has the form of a transport equation

$$y_t = -\frac{\partial J_s^{\nabla K_s}}{\partial x} = -B\left\{\left(1 + y_x^2\right)^{-1/2}\left[\left(1 + y_x^2\right)^{-3/2} y_{xx}\right]_x\right\}_x. \tag{2.1}$$

$J_s^{\nabla K_s}$ and B are given in (1.4) and (1.5).

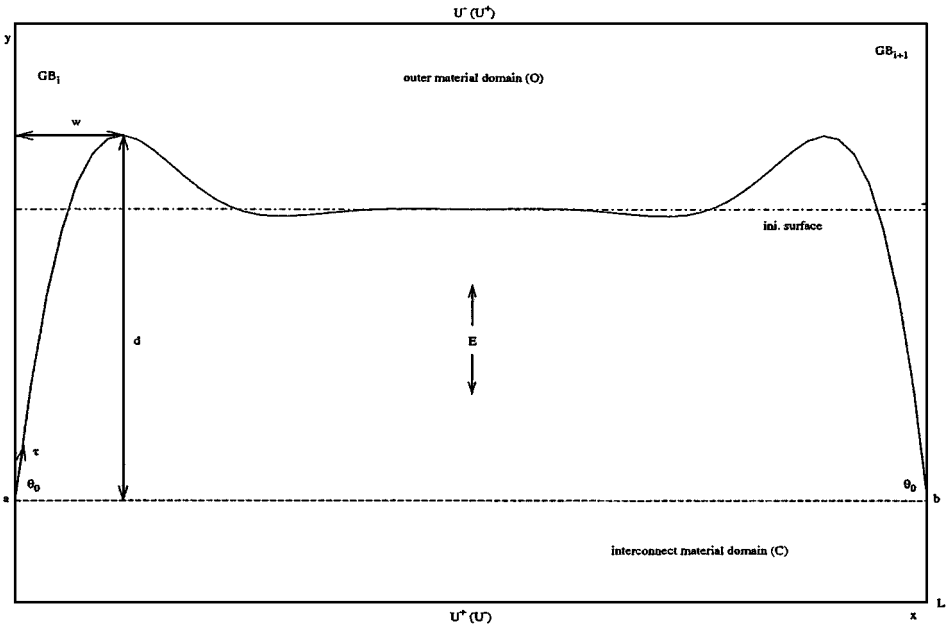

FIG. 1. Sketch of a GB groove. w denotes the half-width of the groove, and d denotes the depth.

For an isolated GB at $x = 0$, the groove continues to develop because the material continues to move from the curved shoulder of the groove to the flat surface. The classical description is provided by an analytic solution (on the $x > 0$ side) of the linearized version of Eq. (2.1) (the "small slope approximation," SSA). The linearized equation has the form [17]

$$y_t = -By_{xxxx}, \tag{2.2}$$

subject to the initial condition

$$y(x, 0) = \text{const}, \tag{2.3}$$

and the boundary conditions

$$\begin{aligned} y_x(0, t) = \tan\theta_0 &= m \ll 1, \\ J_s^{\nabla K_s}(0, t) &= y_{xxx}(0, t) = 0, \\ y(x \to \infty, t) &= \text{const} \quad \text{with all derivatives.} \end{aligned} \tag{2.4}$$

The first condition in (2.4) is the small slope approximation itself. The second one reflects the absence of a GB flux J_{gb}. The solution describes a profile with a constant shape whose linear dimensions are increasing all the time.

Although this analytical approach describes some basic phenomena in interconnects, it is of limited use because of the restriction on the steepness of the slope. There are several numerical techniques which are widely used in modeling moving fronts, such as the *marker/string* (M/S) methods [26] or the *volume-of-fluid* (VOF) methods [7, 20]. These methods deal directly with the evolution equation of type (2.1), and therefore are "explicit"

methods. The M/S methods derived from a Lagrangian approach to front evolution problems. In the Lagrangian approach, the grid is attached to the moving front. A known drawback of the Lagrangian approach is that it is not well suited to computation of bifurcating fronts. In addition, stability and local singularity problems are emphasized more in these methods than in methods based on an Eulerian approach, such as the VOF method. The Eulerian approach,where the front moves through a grid which is fixed in space, does not have these drawbacks, but—as is known—here the fronts are diffused. In addition, some intricate (subcell) bookkeeping is required to properly keep track of fronts.

There are numerical approaches which are based on *finite-element* discretization of the computational region [5]. However, they result in complicated algorithms which involve many computational steps such as computations of the following: displacement field of material points from a reference configuration, the stress field as a result of diffusion in the solid, and geometry update of interfaces. In addition, the computational complexity grows because higher resolution is required as the shape of the interface becomes more complicated. As a result, these methods are unable to handle very complex multidimensional boundary shapes.

2.2. *The Proposed Solution: Use of the Level Set Method*

To "capture" the interface (rather than to track it), our method of choice is the "implicit" LS method. The method was introduced by Osher and Sethian and was further developed during the past several years (for an introduction to the LS methods and an exhaustive bibliography list, see the monographs by Sethian [27, 28]). The method makes it possible to capture drastic changes in the shape of curves (interfaces) and even topology changes.

The basic idea of the method consists of embedding the curve $y(x, t)$ into a higher dimensional space. As a matter of fact, we consider the evolution of a two-dimensional field $\phi(x, y, t)$ such that its zero level set, $\phi(x, y, t) = 0$, coincides with the curve of interest, $y(x, t)$, at any time moment t. The level set function $\phi(x, y, t)$ can be interpreted as a signed distance from the curve $y(x, t)$, which moves in the direction normal to itself.

The evolution of $\phi(x, y, t)$ is described by an Hamilton–Jacobi-type equation. A remarkable trait of the method is that the function $\phi(x, y, t)$ remains smooth, while the level surface $\phi = 0$ may change topology, break, merge, and form sharp corners as ϕ evolves. Thus, it is possible to perform numerical simulation on a discrete grid in the spatial domain and to substitute finite-difference approximation for the spatial and temporal derivatives in time and space.

The evolution equation has the form

$$\phi_t + F|\nabla\phi| = 0, \quad \text{given } \phi(x, t = 0). \tag{2.5}$$

The normal velocity, F, is considered to be a function of spatial derivatives of $\phi(x, y, t)$. In many applications, F is a function of the curvature, K_s, and its spatial derivatives. The curvature K_s may be computed via the level set function ϕ as

$$K_s = \nabla \cdot \mathbf{n}, \quad \mathbf{n} = \frac{\nabla\phi}{|\nabla\phi|} = \left(\frac{\phi_x}{\left(\phi_x^2 + \phi_y^2\right)^{1/2}}, \frac{\phi_y}{\left(\phi_x^2 + \phi_y^2\right)^{1/2}} \right). \tag{2.6}$$

Here $\mathbf{n}$ is "normal vector," and it coincides with the (previously introduced) unit normal to

the surface, $y(x,t)$, on the zero level set $\phi = 0$. Formulas (2.6) can be combined as

$$K_s = \nabla \cdot \frac{\nabla\phi}{|\nabla\phi|} = \frac{\phi_{xx}\phi_y^2 - 2\phi_x\phi_y\phi_{xy} + \phi_{yy}\phi_x^2}{\left(\phi_x^2 + \phi_y^2\right)^{3/2}}, \tag{2.7}$$

and the sign of K_s is chosen such that a sphere has a positive mean curvature equal to its radius. In the case of surface diffusion in 2D,

$$F = -BK_{\tau\tau}^s. \tag{2.8}$$

One drawback of the LS method stems from its computational expense. Its complexity seems to be as many as $O(n^2)$ operations per time step, which is more than any Lagrangian method, which necessitates $O(n)$ operations per time step, where n is the number of grid points in the spatial direction. It is possible, however, to reduce the complexity of the LS method to $O(n)$ using a local (another term is narrow band (tube)) approach [1, 24]. This is achieved by the construction of an adaptive mesh around the propagating interface. We distinguish between the "near field," which is a thin band of neighboring level sets around the propagating front, and the "far field," which contains the rest of the grid points. The evolution equation is solved only in the near field. The values of ϕ at grid points in the far field are not updated at all. When the interface in motion reaches the edge of the narrow band, a new narrow band is built around the current interface position. Note that this could be done without interface reconstruction from the level set function (which requires some additional computations).We just have to examine the shift in the sign of ϕ at grid points adjacent to the interface. The width of the narrow band is determined as a balance between the computation involved in the rebuilt and the calculations performed on far away points.

In most of the applications of the LS method to date, the driving forces were proportional to the curvature (see [27, 28] for review and discussion). There are only a few applications [2, 6, 15] where the driving force is proportional to the *second directional derivative* of the curvature (in the 3D case, to the surface Laplacian of curvature which is constructed from the derivatives in each principal direction), which is the case for the normal velocity function (2.8). Therefore, the present materials science problem presents a rather new (from the mathematical point of view) application for the LS method. As pointed out in [6], "this is an intrinsically difficult problem for three reasons. First, owing to the lack of a nice maximum principle, an embedded curve need not stay embedded, and this has significant implications in attempting to analyze motion which results in topological change. Second, the equations of motion contain a fourth derivative term, and hence are highly sensitive to errors. Third, this fourth derivative term leads to schemes with very small time steps."

2.3. *Computational Algorithm*

A typical computational domain is a rectangular box $[0, l_1; 0, l_2]$ of a material in 2D. The proposed computational algorithm consists of the following steps:

BEGIN ALGORITHM

1. Discretization. The entire computational region W is discretized using a uniform grid $x_i = i\Delta x, y_j = j\Delta y, i = 0 \ldots N, j = 0 \ldots M$, where N and M are the number of grid points in x- and y-directions respectively. The functions are projected on this grid so that $\phi(x,y,t) = \phi_{i,j}(t)$.

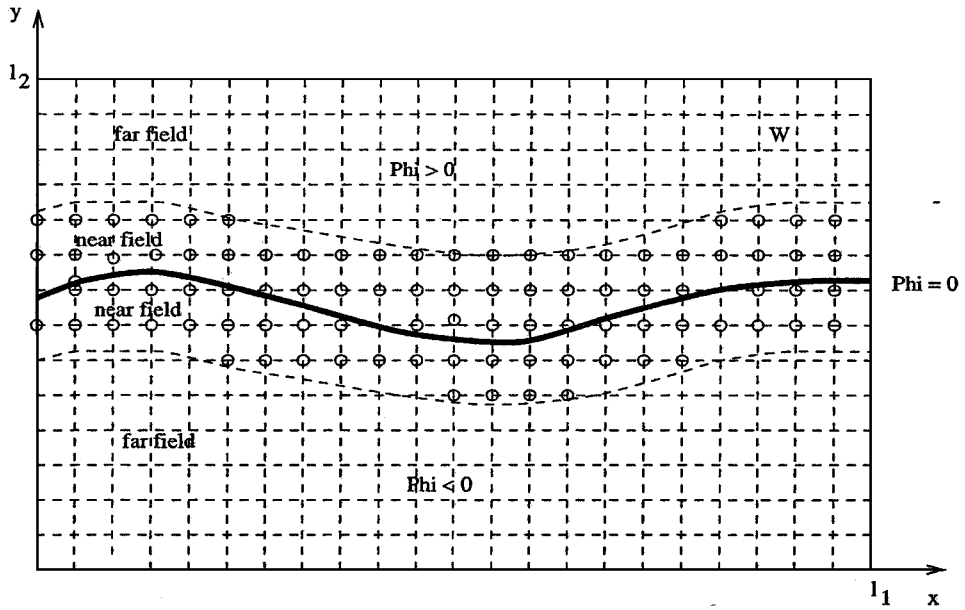

FIG. 2. Computational domain.

2. Initialization. The initial interface, $y(x, t = 0)$, is defined analytically, or as a set of points in W (the points lie on $x =$ const. grid lines, but not necessarily on $y =$ const. grid lines). In the latter case, we define a cubic spline $\xi(x, t = 0)$ passing through these points to perform further initializations. The function $y(x, t = 0)$ need not be necessarily smooth (i.e., it may feature sharp corners, discontinuities, etc.), but in our implementation it must be single-valued to make it possible to choose the sign of ϕ (below).This is because we are only interested in the particular case of analyzing the motion of open curves which may be described by functions during the whole process of the evolution.

We also define the near field and the far field. The width of the near field is usually 5 to 10 grid levels (points).

In the region W, the level set function ϕ is initialized as an exact signed distance function to the initial interface (see Fig. 2),

$$\begin{aligned} \phi(x_i, y_j, t = 0) &< 0 \quad \text{if } y_j < y(x, t = 0) \\ \phi(x_i, y_j, t = 0) &= 0 \quad \text{if } y_j = y(x, t = 0) \\ \phi(x_i, y_j, t = 0) &> 0 \quad \text{if } y_j > y(x, t = 0). \end{aligned} \tag{2.9}$$

Since $\phi(x, y, t = 0)$ is a signed distance function, $|\nabla\phi(x, y, t = 0)| = 1$.

3. Compute normal vector components and curvature using formulas (2.6) and (2.7). The derivatives in (2.6) and (2.7) (as well as in other functions of x and y except the gradient term in the evolution equation itself; see step 6) are discretized using the standard second-order-accurate central difference approximations. Fourth-order-accurate approximations were also tested, but we did not observe any particular increase in the global accuracy of the calculations. In addition, in this case, the implementation of the boundary conditions with the level set function is problematic because of the use of a wide stencil. The time step also

needs to be reduced to have stability. We find that the standard central difference scheme works well for us.

4. Compute first directional derivative of the curvature, K^s_τ,using the formula (1.3) and second directional derivative of the curvature, $K^s_{\tau\tau}$,

$$K^s_{\tau\tau} = \nabla[\nabla K_s \cdot \tau] \cdot \tau = \frac{-K^s_{xx}\phi_y^2 + 2K^s_{xy}\phi_x\phi_y - K^s_{yy}\phi_x^2}{\phi_x^2 + \phi_y^2} + \frac{K_s\left(K^s_x\phi_x + K^s_y\phi_y\right)}{\left(\phi_x^2 + \phi_y^2\right)^{1/2}}$$

$$= \frac{-K^s_{xx}\phi_y^2 + 2K^s_{xy}\phi_x\phi_y - K^s_{yy}\phi_x^2}{\phi_x^2 + \phi_y^2} + K_s\left[K^s_\tau + K^s_y(n_x + n_y) - K^s_x(n_y - n_x)\right]. \quad (2.10)$$

We now have the normal velocity function (2.8) and the flux (1.4).

5. Choose time step. The CFL condition for the surface diffusion is

$$\Delta t_1 \le \min^4(\Delta x, \Delta y)/B. \quad (2.11)$$

The CFL condition for the Hamilton–Jacobi equation in updating the velocity is

$$\Delta t_2 \le \min(\Delta x, \Delta y)/F_{max}, \quad (2.12)$$

where F_{max} is the largest magnitude of the normal velocity in the computational domain. The adaptive time step Δt is chosen as the smaller of the two.

6. Compute backward and forward gradient functions; **update** ϕ from the evolution equation using explicit time-stepping scheme. The solutions of Eq. (2.5) are often only uniformly continuous with discontinuous derivatives, no matter how smooth the initial data [22, 23]. Simple central differencing is not appropriate here to approximate the spatial derivatives in $|\nabla\phi|$. Instead, we use essentially nonoscillatory (ENO) type schemes for Hamilton–Jacobi equations as developed in [22, 23, 29]. More precisely, we use second-order ENO scheme given explicitly in [33]. To update ϕ for one time step, the simplest method is to use Euler, i.e.,

$$\phi^{n+1} = \phi^n + \Delta t L(\phi^n), \quad (2.13)$$

where $L(\phi)$ is the spatial operator in (2.5).

7. Update near field. Check the sign of ϕ at the grid points adjacent to the interface and compute the new locations of near field points.

Go to step 3

END ALGORITHM

Remark 1. To achieve a uniformly high-order accuracy in time, we replace (2.13) with the second-order total variation diminishing (TVD) Runge–Kutta-type discretization [23, 29], which reads

$$\begin{aligned} \tilde{\phi}^{n+1} &= \phi^n + \Delta t L(\phi^n) \\ \phi^{n+1} &= \phi^n + \frac{\Delta t}{2}[L(\phi^n) + L(\tilde{\phi}^{n+1})]. \end{aligned} \quad (2.14)$$

The necessary changes to the algorithm are obvious. The choice of such a low-order Runge–Kutta scheme is justified by the fact that the time step, dictated by stability requirements, is very small.

Remark 2. It is highly desirable that the level sets behave nicely, in the sense that two different level sets do not cross, and in fact remain roughly evenly spaced in time. In terms of the level set function ϕ, this corresponds to the fact that the gradient of ϕ at any given point of a level set does not change dramatically over time. For the numerical method this translates into numerical stability. The best way to achieve this is to keep ϕ close to the signed distance function (or even to keep it exactly equal to the signed distance function), thus keeping $|\nabla\phi| \approx (=)1$. The operations performed on ϕ that accomplish this are called "reinitialization." To summarize, reinitialization is the process of replacing $\phi(x, y, t)$ with another function $\tilde{\phi}(x, y, t)$ that has the same zero contour as $\phi(x, y, t)$ but behaves better, and then taking this new function $\tilde{\phi}(x, y, t)$ as the initial data to use until the next round of reinitialization. There are several ways to do this. The straightforward one (first proposed in [16] and recently used in [2]) is to interrupt the time stepping, reconstruct the interface using some interpolation technique, and directly compute a new signed distance function to the interface. This approach is very expensive and also may bring some undesirable side effects, such as oscillations in the curvature. Instead, we use the iteration procedure of [30]. The function ϕ is reinitialized by solving the Hamilton–Jacobi-type equation to its steady state, which is the desired signed distance function,

$$\phi_t = S(\phi_0)\,(1 - |\nabla\phi|)\,, \tag{2.15}$$

where S is a smoothed sign function,

$$S(\phi_0) = \frac{\phi_0}{\sqrt{\phi_0^2 + \epsilon^2}}, \quad \epsilon = \min(\Delta x, \Delta y). \tag{2.16}$$

The same second-order ENO and TVD Runge–Kutta schemes used for the solution of Eq. (2.5) are used for the iteration of (2.15). As a rule, three or four iterations are sufficient to evolve ϕ close enough to the desired signed distance function. An important practical question is how frequently the reinitializations are applied. In some applications of the level set method, the reinitializations could be triggered after a fixed number of time steps. However, we achieved the best results by reinitializing every time step in the band of level sets that contains points from the near field.

Remark 3. The evolving interface touches the vertical boundaries $x = 0, x = l_1$ at its ends and therefore any boundary conditions imposed on vertical walls influence the evolution of the front. This is why, depending on the nature of the problem, we choose either periodic boundary conditions at vertical walls or only an approximation of the derivatives at vertical walls by one-sided differences. At the horizontal walls, we always use one-sided differences. For illustration purposes, in Fig. 3 we present part of the cosine curve evolving under (2.5) with the speed function $F = -0.1K_{\tau\tau}^s$. Boundary conditions at vertical walls are periodic. Note that the speed of evolution slows as the curve approaches equilibrium state with $K_s = 0$ (line $y = 0.5$). This is because the curvature, and hence its derivative, becomes smaller. To demonstrate the abilities of the method, in Fig. 4 we present the evolution of a nonsmooth curve (step function) under the same speed law.

Remark 4. The very special feature of the presented implementation of the level set method is the incorporation of physical boundary conditions into the level set numerical scheme. Most of the implementations known so far lack this complication. Usually only

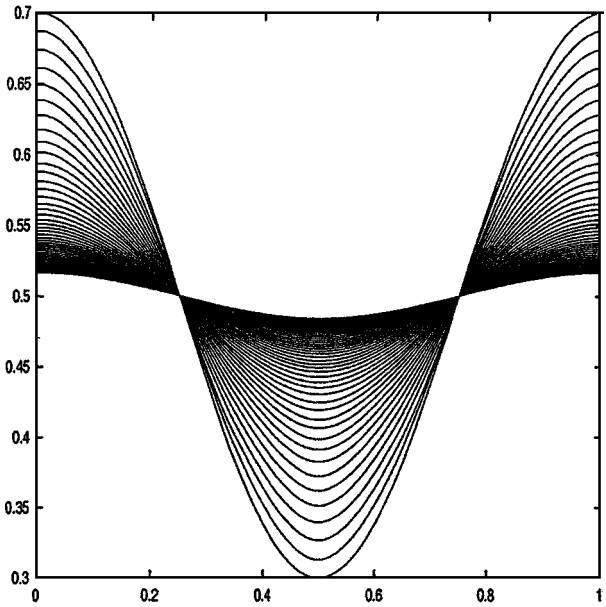

FIG. 3. The cosine curve, evolving under (2.5) with $F = -0.1\ K^s_{\tau\tau}$. A coarse 75×75 grid is used. 25,000 time steps were made by the Runge–Kutta integrator (the shape is printed out every 500 steps), and we reinitialize in every step.

closed interfaces far away from any boundaries domains are considered, while the evolution proceeds far away from the boundaries.

For GB grooving by surface diffusion, two boundary conditions at the groove root are essential: these are conditions of type (2.4), reflecting the fixed slope of the interface and the absence of GB atomic flux. The boundary conditions we impose at $x = l_1$ are zero slope

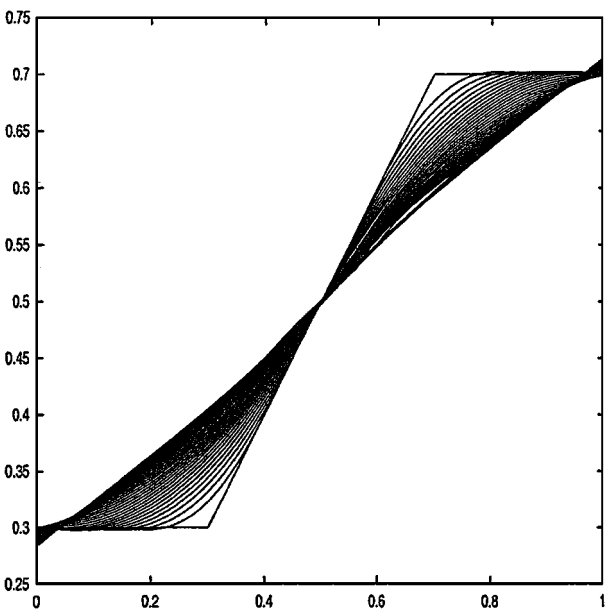

FIG. 4. The evolution of a nonsmooth curve (step function). The grid used is 100×100; 20,000 time steps were made.

of the interface and zero flux. The first condition echoes the initial flat interface. The second condition guarantees the conservation of matter, i.e., a constant area under the groove profile during the evolution.

Special attention was given to the treatment of these boundary conditions within the framework of the level set method. Two methods were developed.

The simplest technique is the use of correction step in the iterative algorithm. The fixed slope at the groove root is achieved in the following way: at every time step, the interface is reconstructed from the ϕ field and the locations of the two end points of the interface (at $x = 0$ and $x = l_1$, respectively) are corrected to preserve the small-slope and the zero-slope conditions.Then, for all grid points that lie on grid lines $x = 0$ and $x = l_1$, it is sufficient to directly compute a new signed distance to the updated locations of the interface end points. This way we incorporate the new locations of the end points back into the ϕ field. This direct reinitialization is performed only for a few grid points that lie on vertical boundaries and, besides, this computation does not contain an iteration loop. The zero-flux conditions could be imposed locally, i.e., in the vicinity of the groove root and of the interface end point at $x = l_1$, or along the the entire $x = 0$ and $x = l_1$ grid lines. After the computed values of K^s_τ are reset to zero, the $K^s_{\tau\tau}$ is computed according to Eq. (2.10), where $K^s_\tau = 0$ at $x = 0, l_1$ and $K^s_\tau \neq 0$ otherwise. After multiplication by $-B$, this gives the values of the normal velocity function (2.8), corrected by the zero-flux constraint.

Extension of the ϕ field beyond the GB makes use of Taylor expansion up to second order (also see Eq. (2.6)),

$$\phi_{-1,j} = \phi_{0,j} - \phi_x\big|_{0,j}\ \Delta x = \phi_{0,j} - |\nabla\phi_{0,j}|\ n_x\big|_{0,j}\ \Delta x = \phi_{0,j} + |\nabla\phi_{0,j}|\sin\theta_0\ \Delta x, \tag{2.17}$$

where $\phi_{-1,j}$ is one grid point beyond the GB. Equation (2.17) incorporates the groove root angle. Then we compute in (2.7) the curvature values, $K^s_{0,j}$, along the GB, using both the values of ϕ inside the computational domain ($\phi_{1,j}$) and outside ($\phi_{-1,j}$). This also gives us the values of $K^s_y\big|_{0,j}$. The zero-flux condition is applied using Eq. (1.3), which, after substitution of normal vector components from (2.6)and rearrangement of the terms, becomes

$$K^s_x\big|_{0,j} = \frac{K^s_\tau|\nabla\phi| + K^s_y\phi_x}{\phi_y}\Big|_{0,j} = -K^s_y\big|_{0,j}\tan\theta_0. \tag{2.18}$$

Applying Taylor expansion again, we get the ghost values of the curvature,

$$K^s_{-1,j} = K^s_{0,j} - K^s_x\big|_{0,j}\ \Delta x, \tag{2.19}$$

where $K^s_x\big|_{0,j}$ is given by (2.18). Now all the data are known and we can compute the values of $K^s_{\tau\tau}$ from (2.10) and the values of the normal velocity from (2.8).

Both methods were used successfully in calculations.

3. NUMERICAL RESULTS: MULLINS PROBLEM

Figures 5 to 7 show the groove profile with different slopes at the groove root, evolving under (2.5) with a speed function $F = -BK^s_{\tau\tau}$. We take $B = 0.025$. The profile is symmetric with respect to the GB at $x = 0$; therefore only its right part is calculated. The results obtained by means of the LS method are shown with solid lines, while reference results for Mullins

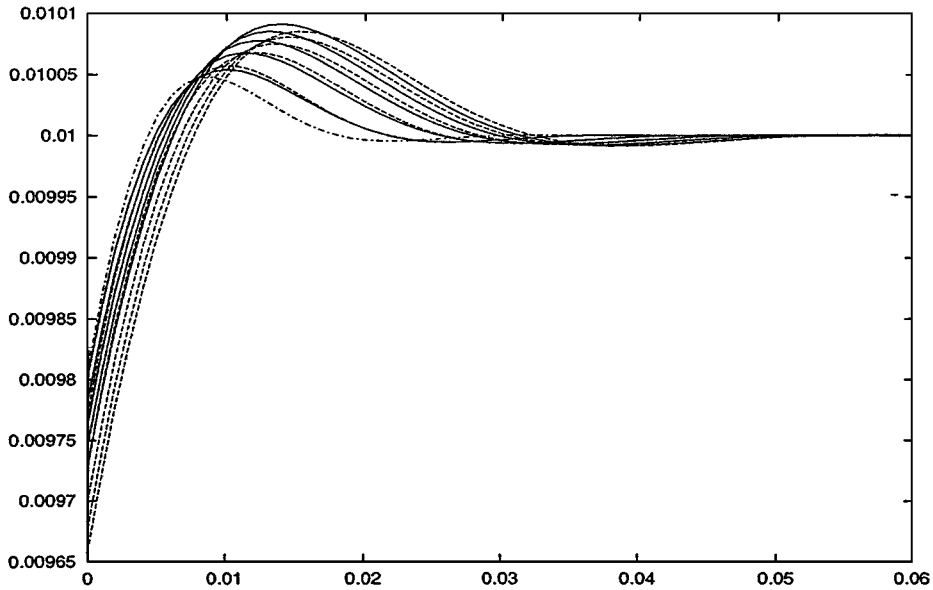

FIG. 5. GB grooving by surface diffusion. The slope at groove root is $m = 6.55e$–02. The initial interface is shown with dashed–dotted line. The numerical results obtained by means of the LS Method are shown with solid lines. The reference results of [17] are shown with dashed lines.

problem (2.2)–(2.4) are shown with dashed lines. In all the three numerical experiments reported here, the dimensions of the computational box are [0., 0.08; 0., 0.02], and the mesh is 120×40.

Our initial interface for the level set simulations already has the shape of Mullins groove. The reason we do not have a flat interface $y(x, 0) = \text{const.}$ as an initial condition is that the

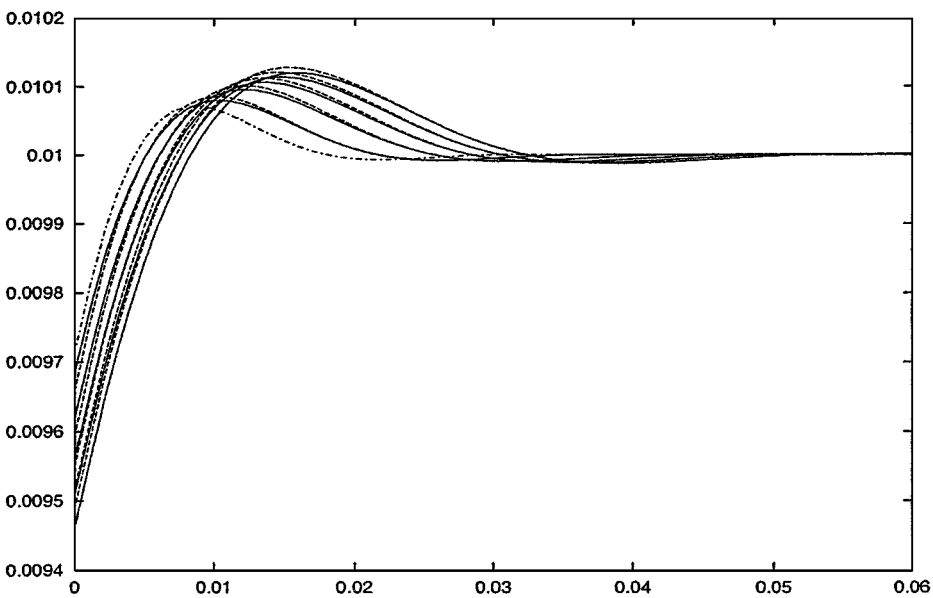

FIG. 6. GB grooving by surface diffussion. The slope at groove root is $m = 9.85e$–02.

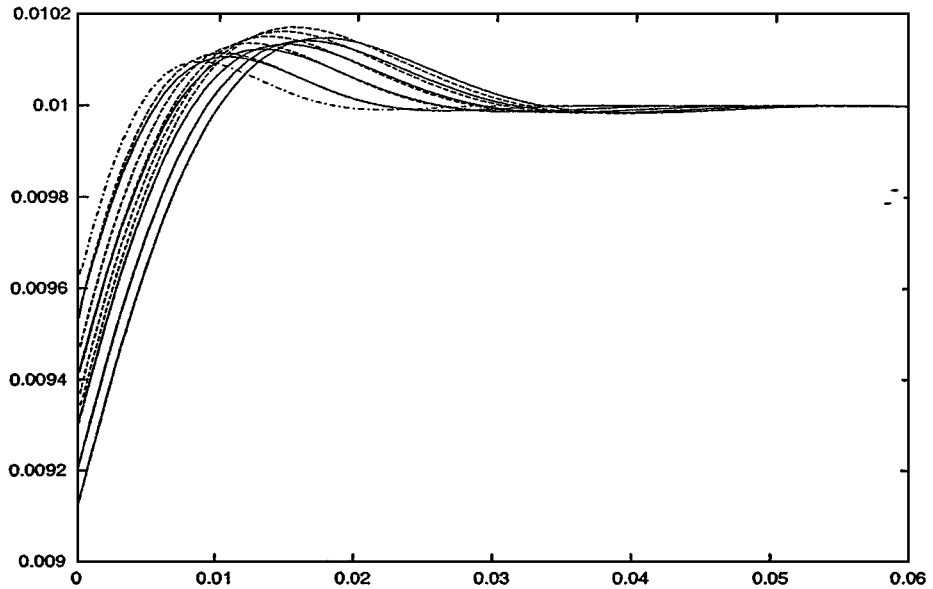

FIG. 7. GB grooving by surface diffusion. The slope at groove root is $m = 1.32e{-}01$.

LS formulation requires a nonzero initial curvature; otherwise, the curve does not evolve at all (since $F = 0$ in this case). The initial interface in Figs. 5–7 is shown with dashed–dotted line.

The initial Mullins groove is obtained as follows: We numerically integrate Eq. (2.2) using the method-of-lines approach. The time integrator is second-order Runge–Kutta and the spatial operator is discretized using second-order central differences. The integration proceeds from $t = 0$ to $t = 8.0e{-}09$. The initial and boundary conditions are given in (2.3) and (2.4), where $\theta_0 = \pi/48, \pi/32,$ and $\pi/24$ represent Figs. 5–7, respectively. The corresponding slopes are $m = 6.55e{-}02, 9.85e{-}02,$ and $1.32e{-}01$. The practical values used in the experiments lie between 0.05 and 0.2 and the range of the groove depths in experiments is between 0.1 and 1 μm. The reason we anticipate the use of the analytic solution to the Mullins problem (2.2)–(2.4) (if it exists) is the truncation of infinite series in which this solution is represented. The reference results for later times are also obtained using the described numerical procedure.

In [17], two kinetic laws were established (within the framework of the SSA). One concerns the evolution of the depth of the groove with respect to the maximum surface elevation (see Fig. 1). The depth, d, is governed by

$$d = 0.973\, m(Bt)^{1/4}. \tag{3.1}$$

The other kinetic law concerns the evolution of the distance between the position of the groove root and that of the surface maximum. In the case of the symmetric groove, we call it the half-width, w, of the groove. It is governed by

$$w = 2.3(Bt)^{1/4}. \tag{3.2}$$

TABLE I
Our Results for GB Grooving, Compared with Classical Mullins Results

Step	t	d, Eq. (3.1)	d, LS M.	w, Eq. (3.2)	w, LS M.	w/d, Eq. (3.3)	w/d, LS M.
0	8.0e–9	2.39e–4	2.39e–4	8.60e–3	8.60e–3	3.60e+1	3.60e+1
2e+3	1.6e–8	2.85e–4	2.50e–4	1.03e–2	1.01e–2	3.60e+1	4.03e+1
4e+3	2.4e–8	3.15e–4	2.68e–4	1.14e–2	1.08e–2	3.60e+1	4.02e+1
6e+3	3.2e–8	3.39e–4	2.84e–4	1.22e–2	1.13e–2	3.60e+1	3.99e+1
8e+3	4.0e–8	3.58e–4	2.99e–4	1.29e–2	1.19e–2	3.60e+1	3.96e+1
10e+3	4.8e–8	3.75e–4	3.13e–4	1.35e–2	1.23e–2	3.60e+1	3.94e+1
12e+3	5.6e–8	3.90e–4	3.26e–4	1.41e–2	1.28e–2	3.60e+1	3.91e+1
14e+3	6.4e–8	4.03e–4	3.38e–4	1.45e–2	1.32e–2	3.60e+1	3.89e+1
16e+3	7.2e–8	4.15e–4	3.50e–4	1.50e–2	1.35e–2	3.60e+1	3.87e+1
18e+3	8.0e–8	4.26e–4	3.61e–4	1.54e–2	1.39e–2	3.60e+1	3.85e+1

Note. The slope at groove root is $m = 6.55e{-}02$.

From these expressions, we have the time-independent ratio

$$w/d = 2.3515/m. \tag{3.3}$$

Under typical experimental conditions a groove of depth $d = 0.3\ \mu$m is formed within $t = 10^4$ s (2.4 h). It is shown in [17] that it would require approximately 8 days to triple this depth. This explains why in our numerical experiments the groove seems to stop developing at later times. The physical reason for this is the increase in the length of a path along which the surface diffusion takes place. As a rule, we stop the run when the groove doubles its depth or width.

For the slopes considered, we observe good qualitative agreement with Mullins solution. The small difference is due to two reasons. First, the results with which we compare are obtained by integrating the linearized equation (2.2), which is, strictly speaking, valid only for infinitesimal slopes. The slopes we choose are, of course, finite, and the governing equation we solve, i.e., Eq. (2.5), is fully nonlinear. Second, there are inevitable area losses, since the LS method is not fully conservative. For bigger slopes, our grooves appear to be deeper and wider than that of Mullins.

In Tables I to III, the results for all the three tests are summarized.

An interesting simple extension of the classical two-grain model is the case of a periodic array of grains separated by parallel GBs. In Fig. 8, we present the results for the evolution of a surface profile intersected by two GBs, i and $i + 1$. The physical boundary conditions at both groove roots are a constant slope of the surface and zero flux (for this example, the slope at groove roots is $m = 9.85e{-}02$). At short times, grooves develop at each grain boundary according to the solution for an isolated grain boundary, as presented in Figs. 5–7; grooving stops when, at sufficiently long times, identical circular arcs develop connecting adjacent GBs. The same result was obtained in [10] using Fourier method and the SSA.

4. THE ELECTROMIGRATION PROBLEM

If an electric field is present, the flux J_s of matter at the curved surface of the conductor is driven simultaneously by curvature gradients and by the component E of the *local* electric

TABLE II

Same as Table I, but the Slope at Groove Root is $m = 9.85e{-}02$

Step	t	d, Eq. (3.1)	d, LS M.	w, Eq. (3.2)	w, LS M.	w/d, Eq. (3.3)	w/d, LS M.
0	8.0e–9	3.59e–4	3.59e–4	8.61e–3	8.61e–3	2.40e+1	2.40e+1
2e+3	1.6e–8	4.29e–4	3.95e–4	1.03e–2	1.03e–2	2.40e+1	2.61e+1
4e+3	2.4e–8	4.74e–4	4.38e–4	1.14e–2	1.13e–2	2.40e+1	2.59e+1
6e+3	3.2e–8	5.10e–4	4.77e–4	1.22e–2	1.21e–2	2.40e+1	2.55e+1
8e+3	4.0e–8	5.39e–4	5.12e–4	1.30e–2	1.29e–2	2.40e+1	2.52e+1
10e+3	4.8e–8	5.64e–4	5.45e–4	1.35e–2	1.36e–2	2.40e+1	2.49e+1
12e+3	5.6e–8	5.86e–4	5.76e–4	1.41e–2	1.42e–2	2.40e+1	2.47e+1
14e+3	6.4e–8	6.06e–4	6.05e–4	1.45e–2	1.48e–2	2.40e+1	2.44e+1
16e+3	7.2e–8	6.24e–4	6.33e–4	1.50e–2	1.53e–2	2.40e+1	2.42e+1
18e+3	8.0e–8	6.41e–4	6.59e–4	1.54e–2	1.58e–2	2.40e+1	2.41e+1

TABLE III

Same as Tables I and II, but the Slope at Groove Root is $m = 1.32e{-}01$

Step	t	d, Eq. (3.1)	d, LS M.	w, Eq. (3.2)	w, LS M.	w/d, Eq. (3.3)	w/d, LS M.
0	8.0e–9	4.80e–4	4.80e–4	8.61e–3	8.61e–3	1.79e+1	1.79e+1
2e+3	1.6e–8	5.74e–4	5.60e–4	1.03e–2	1.06e–2	1.79e+1	1.89e+1
4e+3	2.4e–8	6.36e–4	6.42e–4	1.14e–2	1.19e–2	1.79e+1	1.85e+1
6e+3	3.2e–8	6.83e–4	7.15e–4	1.22e–2	1.30e–2	1.79e+1	1.81e+1
8e+3	4.0e–8	7.22e–4	7.80e–4	1.29e–2	1.39e–2	1.79e+1	1.78e+1
10e+3	4.8e–8	7.56e–4	8.39e–4	1.35e–2	1.47e–2	1.79e+1	1.76e+1
12e+3	5.6e–8	7.86e–4	8.94e–4	1.41e–2	1.55e–2	1.79e+1	1.74e+1
14e+3	6.4e–8	8.12e–4	9.44e–4	1.45e–2	1.62e–2	1.79e+1	1.72e+1
16e+3	7.2e–8	8.36e–4	9.90e–4	1.50e–2	1.69e–2	1.79e+1	1.70e+1
18e+3	8.0e–8	8.59e–4	1.03e–3	1.54e–2	1.75e–2	1.79e+1	1.69e+1

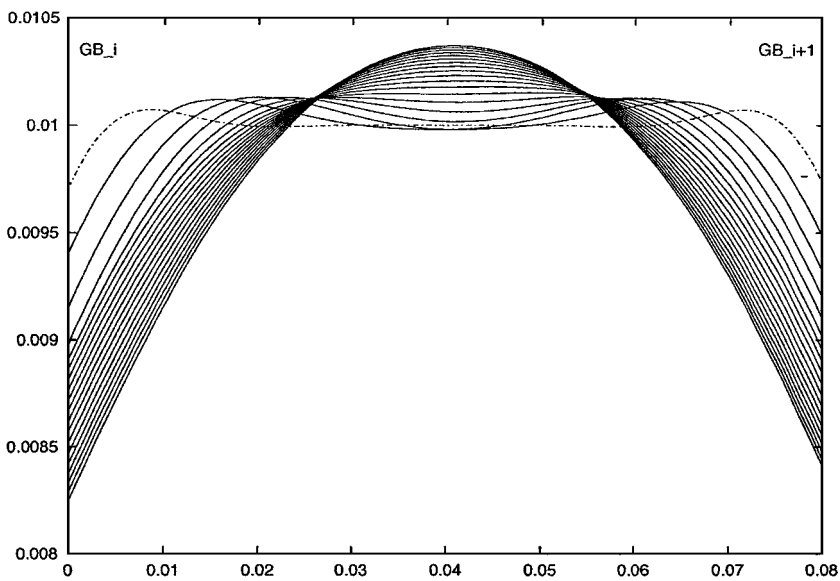

FIG. 8. Long-time evolution of surface profile intersected by two adjacent GBs. The initial surface for LS simulations is shown with dashed–dotted line.

field along the surface. Let C and O denote the conductor (interconnect) material domain and the outer (surrounding) material domain above the surface profile, respectively (see Fig. 1). In a drift velocity (DV) experiment [4], the surface in question represents the cathode edge of the interconnect, while the outer domain is an underlayer with higher resistivity, e.g., TiN. Assume that (at a given time step of overall marching algorithm) $U(x, y)$ is the electric potential within the (rectangular) computational box. $U^-(U^+)$ and $U^+(U^-)$ are its values on the upper and lower boundaries of the box, and U_n is the normal derivative on the boundary. U^- and U^+ are assumed to be time-independent and uniform along the boundaries; $U^+ - U^-$ is the external voltage applied to the interconnect. The distribution $U(x, y)$ is governed by a static elliptic partial differential equation (PDE),

$$\frac{\partial}{\partial x}\left(k\frac{\partial U}{\partial x}\right) + \frac{\partial}{\partial y}\left(k\frac{\partial U}{\partial y}\right) = 0, \tag{4.1}$$

with boundary conditions $U_n = U_x = 0$ on the vertical boundaries of the box (which in our case coincide with GBs). Equation (4.1) is derived from the well-posed three-dimensional potential problem for the two-layer interconnect. The assumptions and complete derivation for the small aspect ratio are presented in [2]. In Eq. (4.1), $k = k(x, y)$ is the specific electrical conductivity (at a given time step) of the material which fills the computational box. To solve (4.1), a finite-difference scheme was developed and analyzed in [2]. The distribution of the specific conductivity in the physical system under consideration is discontinuous: the conductivity inside the conductor material (domain C, Fig. 1) differs by a finite value from that of the surrounding material (domain O). We assume

$$k = \begin{cases} k_{in} = \text{const.} > 0 & \text{if grid point } (x_i, y_j) \in C \\ k_{out} = \text{const.} > 0 & \text{if grid point } (x_i, y_j) \in O, \end{cases} \tag{4.2}$$

i.e., that $k = k(y)$ is a step function. In our numerical experiments we chose the ratio $k_{out}/k_{in} = 0.1$. Since the surface of the conductor evolves in time and space, to find the time-dependent solution $U(x, y, t)$ we need to solve the static equation (4.1) every time step with k given by (4.2). To compute accurately the electric field intensity (which is the derivative of U) the discontinuous distribution of the specific conductivity is smoothed out across the surface profile. The finite-difference discretization of (4.1) in the computational domain leads to a set of linear algebraic equations with a sparse-banded matrix. This set is solved with an effective multigrid iterative procedure [2]. The solution of the previous time step is used as an initial approximation for the current step, which allows fast convergence.

After the potential is established everywhere in the computational domain, the corresponding electrically induced surface flux J_s^E is given by

$$J_s^E = -\frac{D_s \delta_s Z_s}{kT} E = -B_e E, \tag{4.3}$$

where

$$E = -\tau \cdot \nabla U, \tag{4.4}$$

the superscript indicates that the flux is due to the electric field, and

$$B_e = \frac{D_s \delta_s Z_s}{kT}, \tag{4.5}$$

where $Z_s = z_s^* e$ is the effective charge of the ions undergoing electromigration in the surface layer and e is the unit electronic charge; the sign of z_s is usually positive (i.e., matter flux in the direction of the electron flow).

To summarize,

$$J_s = J_s^{\nabla K} + J_s^E, \tag{4.6}$$

where J_s is the total surface flux, and $J_s^{\nabla K}$ is its surface-curvature-driven component. Physically, Eq. (4.6) says that atoms will diffuse in the direction of the electron flow if the field dominates, but toward the position with the large curvature if the surface energy dominates. This competition between the electric field and the surface energy is essential for the groove dynamics.

The electric field also results in the diffusion of matter along GBs. The nonzero diffusion flux along the GB, J_{gb}, in the presence of the electric field is given by

$$J_{gb} = -\frac{D_{gb}\delta_{gb} Z_{gb}}{kT} E, \tag{4.7}$$

where $Z_{gb} = z_{gb}^* e > 0$ is the effective ionic charge, and E is the component of the electric field along the GB. In addition to (1.6), the boundary condition which is due to the electric field reads

$$J_{gb}|_{\text{groove root}} = 2\left(J_s^E + J_s^{\nabla K}\right)|_{\text{groove root}}, \tag{4.8}$$

since both branches of the groove (to the left and to the right from the GB) act as sinks or sources of matter. Obviously, (4.8) reflects the continuity of material fluxes.

With the addition of the electric field, the normal velocity F (see (2.8)) is now changed to

$$F = \frac{\partial J_s}{\partial \tau} = \frac{\partial J_s^{\nabla K}}{\partial \tau} + \frac{\partial J_s^E}{\partial \tau}, \tag{4.9}$$

where J_s is given by (4.6). The details of the calculation of the normal velocity function (4.9) are given in [12].

5. NUMERICAL RESULTS: THE ELECTROMIGRATION PROBLEM

The advance of the surface (front) and GB grooving under combined curvature and electric field effects was simulated for copper interconnects with grain size 0.5 μm at temperature 600 K. The corresponding parameter set is $\Omega = 1.18 \times 10^{-29}$ m^3, $D_s = 3.3 \times 10^{-14}$ m^2/s, $\gamma_s = 1.7$ J/m^2, $kT = 8.28 \times 10^{-21}$ J, $U^+ = -U^- = 5.0 \times 10^{-3}$ V, $k_{in} = 10^8$ $(\Omega\text{m})^{-1}$, $k_{out} = 10^7$ $(\Omega\text{m})^{-1}$, $\delta_{gb} = \delta_s = 3.5 \times 10^{-10}$ m, $z_s^* = z_{gb}^* = 5$, $\theta_0 = \pi/22$. Due to the large number of material parameters involved, we concentrate on the influence of the one which was predicted to greatly affect the grooving process, i.e., the ratio of the

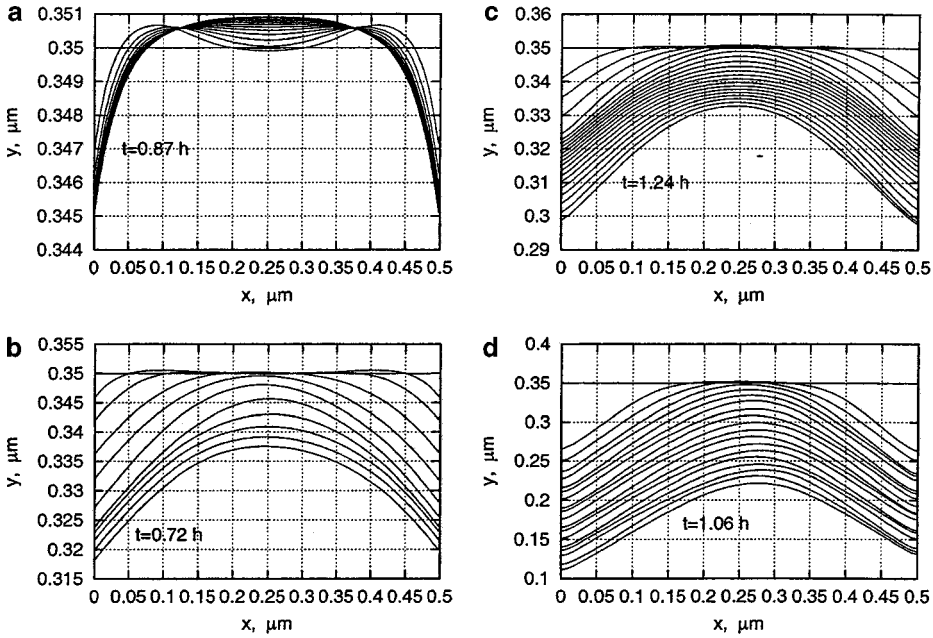

FIG. 9. GB grooving by surface/GB diffusion driven by the surface curvature gradients and the electromigration. (a) $r_d = 0.224$, (b) $r_d = 0.336$, (c) $r_d = 0.561$, (d) $r_d = 22.424$. The surface profiles are dumped every 5000 time steps. The time labels correspond to the (physical) time at which the last profile is dumped.

GB to surface diffusivity, $r_d = D_{gb}/D_s$ [9]. It should be noted that (i) the experimentally measured values of diffusivities could vary, according to different sources, by up to three orders of magnitude, and (ii) D_s can be smaller than D_{gb}, due to, for example, surface contamination, thus giving $r_d > 1$. Typical space–time evolution profiles are shown in Fig. 9. The dimensions of the computational box are $0.5 \times 0.5\ \mu$m (the horizontal dimension being equal to the grain size), and the grid has a 60×60 resolution.

The displacement of the surface with time in Fig. 9 is an accurate illustration of the advancing cathode edge in EM DV experiments. After a transient stage, the displacement velocity V_{em} reaches a constant value, dependent on temperature through an Arhennius-type function,

$$V_{em} = (V_0)_{em} \exp(-E_{em}/kT), \tag{5.1}$$

where $(V_0)_{em}$ is the prefactor and E_{em} is the activation energy. A good match of *both* values between simulation and experiment constitutes a rather rigorous test for the simulation. We have obtained preliminary results for $(V_0)_{em}$ and E_{em}, calculated using the most accurate literature values for both surface and GB diffusivities in copper; these are known at various temperatures through their own Arhennius relationships. For parameter set $(D_0)_s = 0.26 \times 10^{-4}$ m^2/s, $E_s = 0.9$ eV and $(D_0)_{gb} = 0.06 \times 10^{-4}$ m^2/s, $E_{gb} = 0.95$ eV we obtained $(V_0)_{em} = 3.47 \times 10^6\ \mu$m/$h$ and $E_{em} = 0.87$ eV. These calculated values are in excellent agreement with experimental values of $4.6 \times 10^6\ \mu$m/h and 0.94 eV [11], even after we account for some differences, such as grain size and current density. A more detailed report is given in [19]. It appears that the level sets model-based simulation allows, for the first time, an accurate *quantitative* description of DV experiments in polycrystalline lines.

6. CONCLUSIONS

The level set method was used to model the grain-boundary grooving by surface diffusion in an idealized polycrystalline interconnect which consists of grains separated by parallel GBs. The novel feature of the method is the treatment of physical boundary conditions at the groove root. The results obtained are in good agreement with the classical one [17] for the case of an isolated grain boundary (two-grain case) and with more recent results of [10] for the case of periodic array of grains. In addition, the algorithm and its software implementation were used to pursue studies of GB grooving with an arbitrary electromigration flux. Preliminary results for Cu at 600 K show an excellent quantitative agreement of drift velocity preexponent and activation energy between simulation and experiment.

The final time step in the simulations is small. In the Appendix we suggest how to use an implicit approach that can speedup the simulations.

APPENDIX: IMPLICIT STABILIZATION

We assume initially that we have to solve the linear constant coefficient PDE:

$$\frac{\partial \varphi}{\partial t} = -A\Delta^2\varphi. \tag{A.1}$$

An explicit scheme

$$\frac{\varphi^{n+1} - \varphi^n}{\Delta t} = -A\left(\frac{\delta_x^2}{\Delta x^2} + \frac{\delta_y^2}{\Delta y^2}\right)\varphi^n, \quad \varphi^n \equiv \varphi^n_{jk}. \tag{A.2}$$

Von-Neuman (Fourier) stability analysis gives

$$\mu = 1 - 16A\Delta t\left[\frac{1}{(\Delta x)^2}\sin^2\left(\frac{\alpha\Delta x}{2}\right) + \frac{1}{(\Delta y)^2}\sin^2\left(\frac{\beta\Delta y}{2}\right)\right]^2 \equiv 1 - \Delta t A S_{\alpha,\beta}. \tag{A.3}$$

The stability condition requires $|\mu| \le 1$ and the worst case is achieved when the sine terms reach their maximum values of 1.

For the case of $\Delta x = \Delta y$, we get a very severe restriction:

$$\Delta t < \frac{(\Delta x)^4}{32A}. \tag{A.4}$$

Let us add a stabilizing term $M\Delta^2\varphi$ to both sides,

$$\frac{\partial \varphi}{\partial t} + M\Delta^2\varphi = (M - A)\Delta^2\varphi.$$

We discretize in time as

$$\varphi^{n+1} + M\Delta t\Delta^2\varphi^{n+1} = (M - A)\Delta t\Delta^2\varphi^n + \varphi^n,$$

and we get

$$|\mu| = \left| \frac{1 + (M - A)\Delta t S^2}{1 + M\Delta t S^2} \right| \leq 1, \tag{A.5}$$

where S can be the continuous symbol $S = \alpha^2 + \beta^2$ or the discrete $S_{\alpha,\beta}$.

Now as $\Delta x \to 0$ for a fixed Δt the S^2 terms dominate so that $|\frac{M-A}{M}| \leq 1^\circ$, since $M, A > 0$, we need

$$\frac{M - A}{M} \geq -1, \quad 2M \geq A, \quad M \geq \frac{A}{2}.$$

In the linear case, taking $M = \frac{A}{2}(1 + c\Delta t)$ will result in a second-order scheme in time and absolute stability. For the variable A, we will require

$$M \geq \max_{x,y} |A(x, y)|.$$

The Solution Process

Let

$$\varphi^{n+1} + M\Delta^2\varphi^{n+1} = F^n, \tag{A.6}$$

where F^n is known. For the periodic case, we write both φ and F as Fourier expansions

$$\begin{aligned} F_{jk} &= Re \sum_{\alpha,\beta} \tilde{F}_{\alpha,\beta} e^{i(\alpha j\Delta x + \beta k\Delta y)} \\ \varphi_{jk}^{n+1} &= Re \sum_{\alpha,\beta} \tilde{\varphi}_{\alpha,\beta} e^{i(\alpha j\Delta x + \beta k\Delta y)}. \end{aligned} \tag{A.7}$$

We find $\tilde{F}_{\alpha,\beta}$ by FFT and then $\tilde{\varphi}_{\alpha,\beta}$ from the Fourier tranform of Eq. (7.6)

$$\tilde{\varphi}_{\alpha,\beta} \left(1 + M(\alpha^2 + \beta^2)^2\right) = \tilde{F}_{\alpha,\beta},$$

or we may use the numerical $S_{\alpha,\beta}$ which approximates the exact symbol. It is less accurate but avoids some of the Gibbs phenomena. Then each coefficient is obtained by applying the inverse Fourier transform.

REFERENCES

1. D. Adalsteinsson and J. A. Sethian, A fast level set method for propagating interfaces, *J. Comput. Phys.* **118**, 269, (1995).
2. A. Averbuch, M. Israeli, and I. Ravve, Computation for electro-migration in interconnects of micro-electronics devices, *J. Comput. Phys.* **167**, 316 (2001).
3. I. A. Blech and C. Herring, Stress generation by electromigration, *Appl. Phys. Lett.* **29**, 131 (1976).
4. I. A. Blech and E. Kinsbron, Electromigration in thin gold films on Molybdenum surfaces, *Thin Solid Films* **25**, 327 (1975).
5. A. F. Bower and L. B. Freund, Finite element analysis of electromigration and stress induced diffusion in deformable solids, *Mater. Res. Soc. Symp. Proc.* **391**, 177 (1995).

6. D. Chopp and J. A. Sethian, *Motion by Intrinsic Laplacian of Curvature*, UCB PAM Report 746 (1998).
7. A. J. Chorin, Flame advection and propagation algorithms, *J. Comput. Phys.* **35**, 1 (1980).
8. F. Y. Genin, W. W. Mullins, and P. Wynblatt, The effect of stress on grain-boundary grooving, *Acta Metall.* **41**, 3541 (1993).
9. E. Glickman and M. Nathan, On the unusual electromigration behavior of copper interconnects, *J. Appl. Phys.* **80**, 3782 (1996).
10. S. A. Hackney, Grain-boundary grooving at finite grain size, *Scripta Metall.* **22**, 1731 (1988).
11. C.-K. Hu, R. Rosenberg, and K. Y. Lee, Electromigration path in Cu thin-films lines, *Appl. Phys. Lett.* **74**, 2945 (1999).
12. M. Khenner, A. Averbuch, M. Israeli, M. Nathan, and E. Glickman, Level set modeling of transient electromigration grooving, *Comput. Mater. Sci.* **20**, 235 (2001).
13. L. Klinger, E. Glickman, V. Fradkov, W. Mullins, and C. Bauer, Extension of thermal grooving for arbitrary grain-boundary flux, *J. Appl. Phys.* **78**, 3833 (1995).
14. L. Klinger, E. Glickman, V. Fradkov, W. Mullins, and C. Bauer, Effect of surface and grain-boundary diffusion on interconnect reliability, *Mater. Res. Soc. Symp. Proc.* **391**, 295 (1995).
15. Z. Li, H. Zhao, and H. Gao, A numerical study of electromigration voiding by evolving level set function on a fixed cartesian grid, *J. Comput. Phys.* **152**, 281 (1999).
16. R. Malladi, J. A. Sethian, and B. C. Vemuri, Shape modelling with front propagation: A level set approach, *IEEE Trans. Pattern Anal. Mach. Intell.* **17** (1995).
17. W. W. Mullins, Theory of thermal grooving, *J. Appl. Phys.* **28**, 333 (1957).
18. W. W. Mullins, Mass transport at interfaces in single component systems, *Metall. Mater. Trans.* **26A**, 1917 (1995).
19. M. Nathan, M. Khenner, A. Averbuch, and E. Glickman, Electromigration drift velocity in Cu interconnects modeled with Level Sets, *Appl. Phys. Lett.* **77**, 3355 (2000).
20. W. Noh and P. Woodward, A simple line interface calculation, *in Proceedings, Fifth International Conference on Fluid Dynamics* (Springer-Verlag, Berlin, 1976).
21. M. Ohring, Electromigration damage in thin films due to grain-boundary grooving process, *J. Appl. Phys.* **42**, 2653 (1971).
22. S. Osher and J. A. Sethian, Fronts propagating with curvature dependent speed: Algorithms based on Hamilton–Jacobian formulation, *J. Comput. Phys.* **79**, 12 (1988).
23. S. Osher and C. W. Shu, High-order essentially non-oscillatory schemes for Hamilton–Jacobi equations, *J. Numer. Anal.* **28**, 907 (1991).
24. D. Peng, B. Merriman, S. Osher, H. Zhao, and M. Kang, *A PDE Based Fast Local Level Set Method*, UCLA CAM Report 98-25 (1998).
25. R. Rosenberg and M. Ohring, Void formation and growth during electromigration in thin films, *J. Appl. Phys.* **42**, 5671 (1971).
26. J. A. Sethian, Curvature and the evolution of fronts, *Commun. Math. Phys.* **101**, 487 (1995).
27. J. A. Sethian, *Level set Methods: Evolving Interfaces in Geometry, Fluid mechanics, computer Vision and Materials Science* (Cambridge University Press, Cambridge, 1996).
28. J. A. Sethian, Level Set Methods and Fast Marching Methods: Evolving Interfaces in Computational Geometry, Fluid Mechanics, Computer Vision and Materials Science (Cambridge University Press, Cambridge, 1999).
29. C.-W. Shu and S. Osher, Efficient implementation of essentially non-oscillatory shock-capturing schemes, *J. Comput. Phys.* **77**, 439 (1988).
30. M. Sussman, P. Smereka, and S. Osher, A level set approach for computing solutions to incompressible two-phase flow, *J. Comput. Phys.* **114**, 146 (1994).
31. F. G. Yost, Voiding due to thermal stress in narrow conductor lines, *Scripta Metall.* **23**, 1323 (1989).
32. W. Zhang and J. H. Schneibel, Numerical simulation of grain-boundary grooving by surface diffusion, Comput. Mater. Sci. **3**, 347 (1995).
33. H.-K. Zhao, T. Chan, B. Merriman, and S. Osher, A variational level set approach to multiphase motion, *J. Comput. Phys.* **127**, 179 (1996).